NANO LETTERS
Letter
Cite This: Nano Lett. XXXX, XXX, XXX−XXX
pubs.acs.org/NanoLett

Photo-Rechargeable Organo-Halide Perovskite Batteries

Shahab Ahmad,*[†] Chandramohan George,[†] David J. Beesley,[†] Jeremy J. Baumberg,[‡] and Michael De Volder*[†]

[†]Institute for Manufacturing, Department of Engineering, University of Cambridge, Cambridge CB3 0FS, United Kingdom
[‡]Nanophotonics Centre, Cavendish Laboratory, University of Cambridge, Cambridge CB3 0HE, United Kingdom

Supporting Information

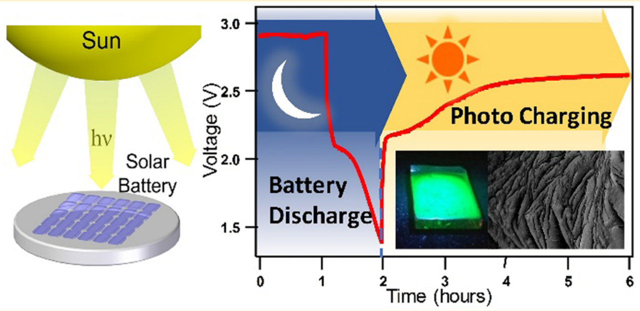

ABSTRACT: Emerging autonomous electronic devices require increasingly compact energy generation and storage solutions. Merging these two functionalities in a single device would significantly increase their volumetric performance, however this is challenging due to material and manufacturing incompatibilities between energy harvesting and storage materials. Here we demonstrate that organic−inorganic hybrid perovskites can both generate and store energy in a rechargeable device termed a photobattery. This photobattery relies on highly photoactive two-dimensional lead halide perovskites to simultaneously achieve photocharging and Li-ion storage. Integrating these functionalities provides simple autonomous power solutions while retaining capacities of up to 100 mAh/g and efficiencies similar to electrodes using a mixture of batteries and solar materials.

KEYWORDS: *Metal halide perovskite, layered-materials, Li-ion battery, photobattery, self-rechargeable*

The Internet of things (IoT), smart cities, and other autonomous connected devices require continuous remote power sources for sensing, data processing, and communication.[1−6] To date, these power requirements are typically met by combining solar cells with rechargeable batteries. However, the use of two separate devices results in duplicated components and increased packaging requirements which adds to the device complexity, weight and cost.[7] More fundamentally, this leads to ohmic transport losses and is suboptimal because most solar cells have an open circuit voltage of 0.6 to 1.0 V which is insufficient to charge commercial Li-ion batteries, thus requiring additional dc-to-dc convertors or stacked cells.[8] Ongoing research efforts have improved the packaging efficiency by integrating batteries and solar cells in the same housing, as well as by developing designs where electrodes are shared between the battery and the solar cell.[9−12] These advances in device integration reduce the ohmic transport losses and increase the gravimetric energy density. However, coassembling devices remains an imperfect manufacturing and scientific solution. Going some way to address these issues, photoelectrodes that consist of a physical mixture of solar energy harvesting and Li-ion storage materials have recently been reported.[13,14] Physically mixing photovoltaic and storage materials allows for compact device implementation, but suffers from other fundamental limitations: these include the mismatch of energy levels between the light-absorbing and storage materials resulting in inefficient charge transfer, the blocking of light by the storage medium so that less light reaches the light-absorbing material, reduced charge transport due to poor interfaces between the two materials, and manufacturing challenges such as the phase segregation of the two materials. It is therefore clear that a new material system is needed to address the above issues.

Paolella et al. have recently demonstrated light-assisted delithiation of lithium iron phosphate ($LiFePO_4$) nanocrystals in a two-electrode system where Li-metal is used as anode and a mixture of $LiFePO_4$ and Ru dye (N719) as cathode.[13] In this work, the solar energy harvesting is performed by the dye, and energy storage by $LiFePO_4$, resulting in photoconversion and storage efficiencies of 0.06%. In 2016, Sato et al. demonstrated a single anode material (TiO_2) integrated into a semitransparent battery electrode.[15,16] While this is an elegant solution, TiO_2 only absorbs light in the UV spectrum, and the cyclability, voltage window, and charge retention of these materials is rather limited. Miyasaka et al. reported a combined light conversion and energy storage device using soft carbonaceous materials where the photoactive layer is a thin LiI film deposited on a mesoporous dye-filled TiO_2 film,[11] but the output power of these three-electrode devices in sunlight is only 0.5 mW with an open circuit voltage (OCV) of 0.45 V. To the best of our knowledge, despite the above examples of photobattery effects, the use of a single active material which can perform both photocharging and energy storage processes efficiently has not been reported.

Received: December 7, 2017
Revised: January 25, 2018
Published: February 9, 2018

ACS Publications

DOI: 10.1021/acs.nanolett.7b05153
Nano Lett. XXXX, XXX, XXX−XXX

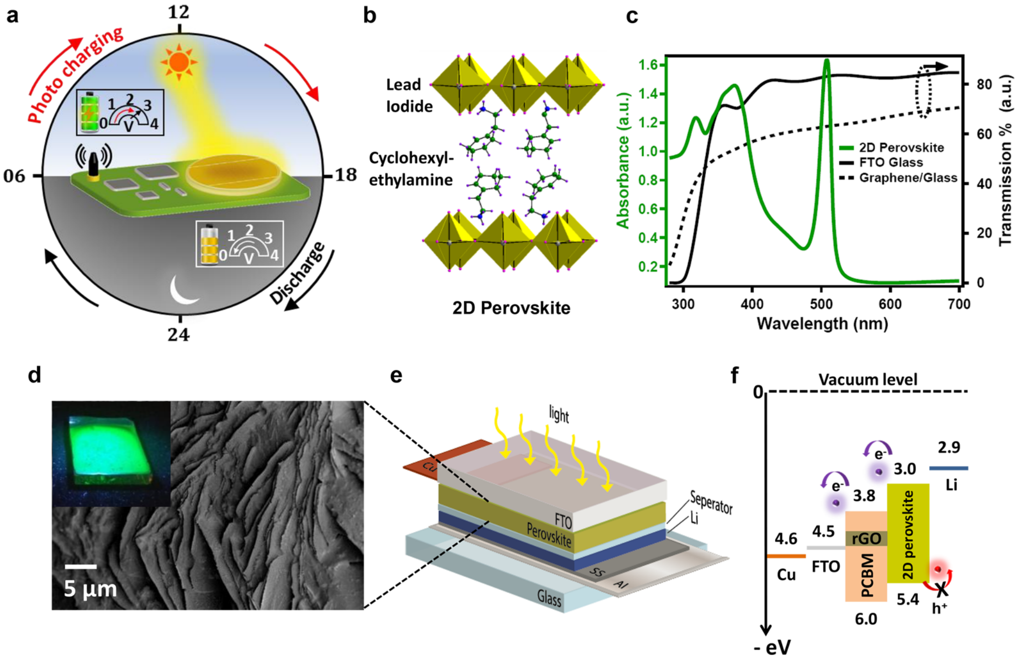

Figure 1. The 2D perovskite and fabrication of photobattery. (a) Schematic representation of the photobattery concept. (b) Crystal structure of 2D layered perovskites (CHPI). (c) Optical absorption spectra of CHPI thin films and transmission of FTO glass and graphene substrates. (d) SEM image of drop-cast 2D perovskite electrodes taken at 45° tilt. The inset shows a PL image of the corresponding perovskite film ($\lambda_{ex} \sim 300$ nm LED source). (e) Schematic and (f) energy level diagram of perovskite photobatteries.

In recent years, three-dimensional (3D) metal halide based perovskites have been studied intensively for use in solar cells because of their high conversion efficiencies of up to 22%.[17−19] More recently, reports have suggested perovskites might also be used as anode materials in Li-ion batteries.[20] However, these functionalities have never been combined in a single solar-battery device. Here we present the first report that polycrystalline metal-halide-based 2D perovskite materials, namely $(RNH_3)_2MX_4$ [R, organic; M, metal; X, halide], can combine both energy storage (battery functionality) and photocharging (photovoltaic functionality) simultaneously (Figure 1a). This integration alleviates the above issues with composite devices and has the potential to open up an entirely new application domain for perovskites. The 2D perovskites are used in this work because they self-assemble into very stable layered structures where inorganic monolayers of corner-sharing $[MX_6]^{4-}$octahedra are confined between interdigitating bilayers of organic cations (Figure 1b).[21] Their enhanced stability compared to 3D systems is important for battery applications but comes at the cost of a lower solar cell efficiency due to the inhibition of out-of-plane charge transport by the organic cations.[22−24] The optical absorption of the $(C_6H_9C_2H_4NH_3)_2PbI_4$ (hereafter CHPI) thin films show a characteristic strong exciton absorption peak at 508 nm with a broad band-to-band absorption around 380 nm (Figure 1c). Photoluminescence (PL) imaging of the perovskite films shows strong green emission from the characteristic room temperature excitonic emission of CHPI (Figure 1d inset, excited with a 300 nm LED source, $\lambda_{PL} \sim 518$ nm).[21]

The application of 2D perovskites for energy storage applications has not been reported previously. Therefore, we start by analyzing the performance of 2D perovskites as a battery material in standard coin cell configurations (see Methods). The morphology of CHPI at the microscale is key for both the battery and solar performance, therefore, instead of using standard spin coating, which results in horizontal stacking of the 2D perovskite platelets (see Supporting Information, Figure S1a,b),[21] we drop-cast the perovskite solution blended with conductive additives (reduced graphene oxide, rGO) and a binder (PVDF) which results in vertically aligned nanoplatelets (~320 nm thick and ~8−10 μm high, Figure 1d and Supporting Information, Figure S1c). Because these vertically aligned perovskite nanoplatelets are grown directly on the surface of the FTO substrate, there is a good interface and charge transfer from the perovskite film to the FTO. Thick films with vertically aligned crystals introduce porosity and improve light interactions when compared to pristine CHPI thin films (transmittance 50% versus 14%, see Supporting Information, Figure S1d). At the same time, rGO improves the electrical transport within the film and PVDF enhances the mechanical stability of the cell. Other carbon-based conductive additives such as carbon nanotubes (CNTs) also produce functioning cells but of poorer cyclability and lower efficiency. A likely reason for the better performance of rGO is the lower work function of rGO (−4.4 eV) compared to CNTs (−4.8 eV) which reduces the energy barrier for photoelectron transport from perovskite to rGO (Figure 1f). XRD measurements (see Supporting Information, Figure S1e,f) show that the presence of rGO in the perovskite film does not affect the intralayer *d*-spacing, which suggests the rGO is located in-between the perovskite crystals. Charge−discharge potential curves of coin cell (nonphoto-chargeable) batteries (see Supporting Information, Figure S2a,b) show that lead−iodide perovskites offer capacities of ~90−100 mAh/g in the first cycle and 2D lead bromide ($(C_6H_9C_2H_4NH_3)_2PbBr_4$, hereafter CHPB) perovskite cells achieve up to ~410 mAh/g, which is higher than the graphite anodes (~370 mAh/g) used in commercial Li-ion batteries. Despite exhibiting useful capacity, these perovskite materials presently suffer from stability issues such that their capacity drops to a fifth of its initial value within

DOI: 10.1021/acs.nanolett.7b05153
Nano Lett. XXXX, XXX, XXX−XXX

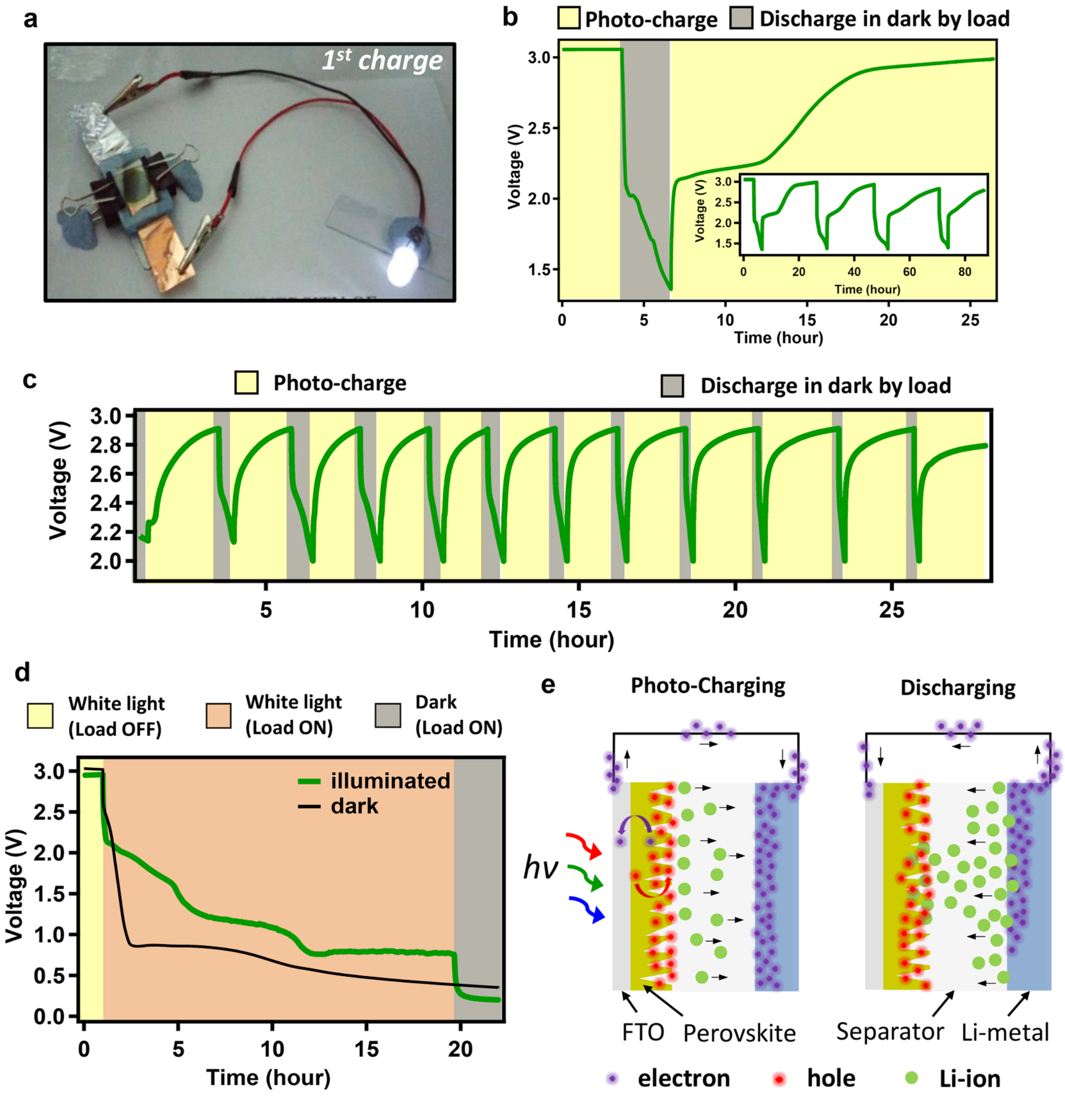

Figure 2. Perovskite photobattery performance and mechanism. (a) Photograph of a 3 V LED powered by a CHPI photobattery after the first cycle of photocharging. (b) First photocharge (broadband light 100 mW/cm^2) and discharge (dark, 21.5 kΩ load) voltage profile of a CHPI-based photobattery. The inset shows further cycling of the photobattery under similar conditions. (c) Photobattery cycling over a limited potential range. (d) Potential discharge curve for photobatteries in dark (black) and illuminated (green) conditions. (e) Schematics of the photocharge generation, transfer, and storage mechanisms in perovskite photobatteries.

a few galvanostatic charge−discharge cycles (see Supporting Information, Figure S2b). This accords with recent reports on nonphoto-rechargeable 3D perovskites batteries.[20] Indeed these stability issues are being addressed intensely by the perovskite community for various other applications.[25]

A hybrid device architecture is designed to achieve the above-mentioned simultaneous solar-battery functionality (Figure 1e). Briefly, a 2D perovskite-rGO-PVDF film is sandwiched between a separator (frit) and a transparent collector electrode (here fluorine-doped tin oxide, FTO, see Methods). For energetically favorable transport of electrons from the perovskite to the electron-selective electrode (Cu-foil), either rGO or PCBM are used as electron transport materials (see Methods and Figure 1f). A mesh-like Cu electrode could be used as an alternative for FTO but this would block part of the light and reduce the overall performance of the device, therefore in our photobattery devices we have used FTO connected by Cu-metal foils, as shown in Figure 1e. Photobatteries are first charged to saturation by a broadband light source (λ ∼ 420−650 nm, intensity ∼100 mW/cm^2, see Supporting Information, Figure S3) and then discharged through an electrical resistor of 21.5 kΩ (or an LED if mentioned). Initially, the photobattery with PCBM as conducting additive (structure **B1**, see Methods) is photocharged up to 3.05 V and then discharged to 0.4 V. However, we found that below 1.4 V the typical dark yellow color of the CHPI electrodes turns black (see Supporting Information, Figure S4a,b). To confirm that the change in color is not due to lithiation of the FTO, it is replaced by graphene, but the color change persists (see Supporting Information, Figure S5). Further, at low discharge voltages, post-mortem Fourier transform infrared spectroscopy (FTIR) suggests excessive electrolyte decomposition or solid electrolyte interphase (SEI) formation (see Supporting Information, Figure S6).[26−28] Therefore, we limit the discharge voltage to 1.4 V in what follows.

Figure 2 shows the photobattery performance in more detail. First, we find that our fully light-charged devices can power a commercial 3 V white light LED (operating at electrical power of ~0.6 mW) for more than an hour (photograph Figure 2a and Supporting Information, Figure S7a). More energy can be stored by simply using larger area electrodes because the photobattery perovskite electrode is insensitive to defects from scaling. Further, these photobatteries can run over the span of a full week, which is encouraging in comparison to the lifetime of other perovskite systems.[29] Because the photobatteries are charged with light and discharged over a resistor, the charge and discharge cycles are very different in terms of current density, and we estimate the Coulombic efficiency (CE) to be 17% in the first galvanostatic charge−discharge tests in the full potential window. Further, we find a drop in voltage of less than 10% over a span of 13 h for photocharged batteries left in dark conditions (see Supporting Information, Figure S7b). When testing the devices between 3.0 and 1.4 V, good cyclability is achieved with only a slight decay in the photocharging potential (Figure 2b, with rGO conducting additive, see **B2** in Methods). When cycled between 2.95 and 2.0 V, no decay in the photocharging potential is observed after more than 10 cycles. However, the capacity of the electrode shows some fading (Figure 2c), as expected based on the initial coin-cell results (see Supporting Information, Figure S2c). Below, we investigate the storage and capacity fading mechanism in more detail. Next, two batteries (structure **B2**) are discharged through identical loads (21.5 kΩ) with the first battery in dark conditions and the second one illuminated (100 mW/cm^2). As shown in Figure 2d, the latter maintains an overall higher output potential along with an almost two times longer discharge time from ~3.0 to 1.4 V. Further, a plateau at ~1.1 V is observed before stabilizing at 0.8 V. At this stage, the battery functionality is depleted, and the device relies only on photogenerated charge carriers (conversion efficiency, η ~ 0.034%). This is confirmed by the sudden drop to 0.2 V when the light is turned off after 19 h (decay time ~14 min, gray region in Figure 2d). This data further confirms the ability of CHPI to simultaneously operate as a battery and a photo harvesting material. Alternative photocharge/discharge curves in light and dark conditions are reported in Supporting Information, Figure S8.

In what follows, we elucidate both the energy storage and the photocharging mechanisms of these devices. As suggested in a recent report of DFT simulations of 3D organic−inorganic hybrid perovskite batteries, we believe that energy is stored in our 2D perovskites by a combination of an intercalation and conversion mechanism.[30] We first study the storage mechanism at low discharge levels using in situ confocal PL measurements (λ_{PL}~ 518 nm, diode laser excitation source, λ_{ex} ~ 447 nm, see Supporting Information, Figure S9). Figure 3a shows that the bright green PL of the photocharged devices is quenched when discharging to 2.26 V, and the exciton PL intensity decreases nonlinearly similar to the potential discharge curve (Figure 2d). These in situ measurements suggest that the discharge process modifies the perovskite structure, which we investigate further by post-mortem X-ray diffraction (XRD) (Figure 3b). These measurements show a shift in the CHPI characteristic (002) plane peak (2θ ~ 5.2°) towards lower diffraction angles for electrodes discharged to 1.85 V or less (2θ ~ 4.9°). This implies that the *d*-spacing between the metal halide atomic interlayers increases from 17 Å for pristine electrodes to 18 Å when discharged to 1.85 V or lower. This expansion in the *d*-spacing suggests that Li-ions are inserted between the metal halide atomic interlayers.[30] The change in *d*-spacing during lithiation also suggests that photocharging is not due to surface

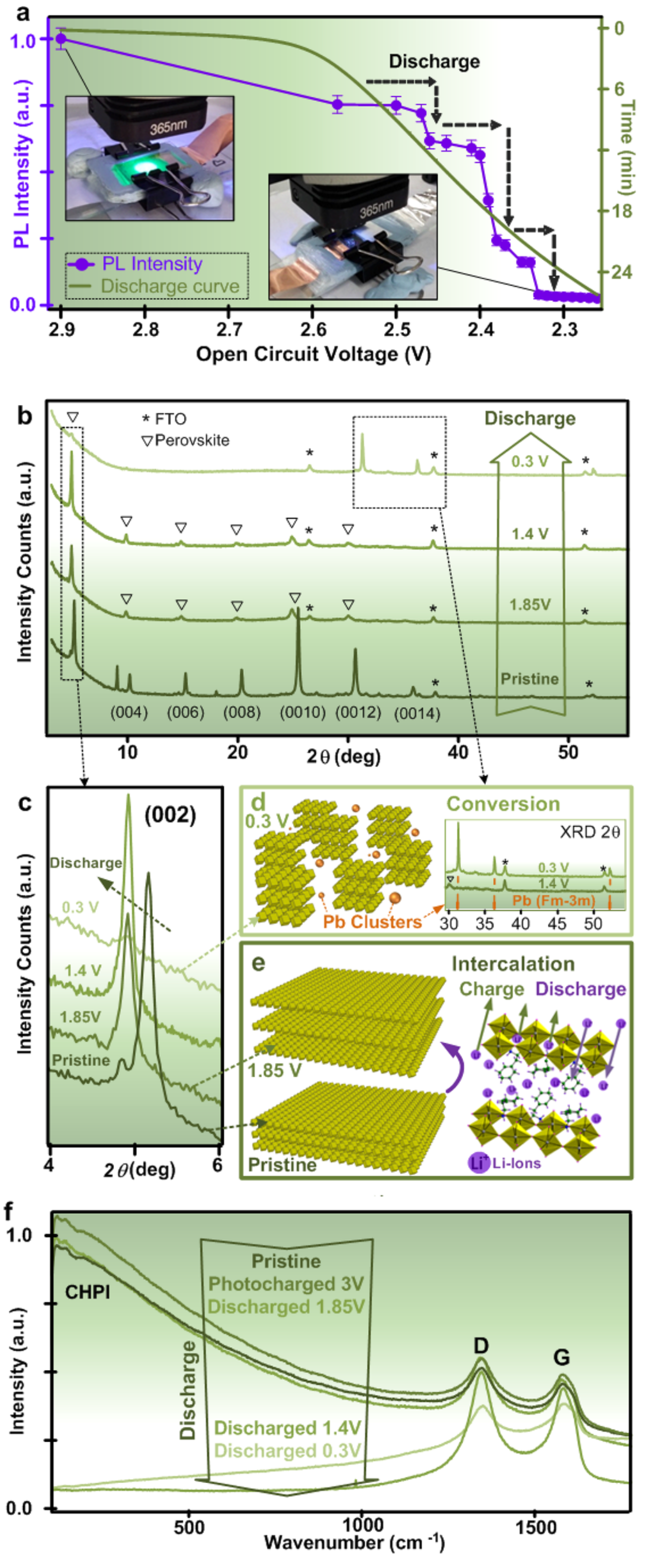

Figure 3. In situ measurements. (a) In situ confocal PL versus measured open circuit voltage while discharging through a resistive load (dashed arrows added to guide the eye). Insets show the PL response (λ_{ex} ~ 365 nm LED source) of the photobattery when photocharged to 2.90 V (left) and after discharge to 2.26 V (right). (b) XRD patterns of photobattery electrodes (**B2**) discharged at different potential levels, with XRD of pristine CHPI thin film also added for comparison (shifted along *y*-axis for clarity). (c) Close-up view of characteristic peak (002) of CHPI, showing a shift toward lower diffraction angle upon lithiation. (d) Schematic representation of Pb-

Figure 3. continued

metal cluster formation in case of perovskite photobattery electrode discharged to deep potential levels. Inset XRD spectra of electrode discharged to 0.3 V matches well with lead metal XRD peaks (space group: $Fm\overline{3}m$ shown in orange). (e) Layered crystal structure of CHPI illustrating increase in *d*-spacing upon Li-ion intercalation between PbI_6 octahedra. (f) Micro-Raman spectra of CHPI electrodes at different discharge levels.

reactions but is a process taking place in the bulk of the perovskite. This Li-ion migration in CHPI can follow different paths (ionic radius ~0.76 Å), for instance through the spaces between lead halide octahedrons (>37 Å^2) along the *c*-axis of the triclinic unit cell of 2D-perovskite crystal[31] (see Figure 3c). This is similar to organic moieties which travel between adjacent PbI_6 octahedrons to form the 2D perovskites crystals[32] during initial intercalation of the organics into PbI_2.

At voltages below 1.4 V, both the perovskite peaks disappear in the XRD patterns (Figure 3b) and in the Raman spectra (Figure 3f), indicating a more substantial change in the material structure. Further, at 0.3 V new XRD peaks appear, which match well with Pb (space group $Fm\overline{3}m$, Figure 3d) and is likely the result of a conversion reaction similar to one suggested recently for 3D perovskites (eq 1):[30]

$$2Li + (C_6H_9C_2H_4NH_3)_2PbI_4 \rightarrow 2(C_6H_9C_2H_4NH_3I) + 2LiI + Pb(m) \tag{1}$$

During the photocharging process, the alternating 2D semiconducting inorganic and insulating organic monolayers act as potential wells and barriers respectively, resulting in electronic and dielectric confinement effects,[33−35] and generation of excitons upon illumination with photons exceeding the exciton energy (λ_x ~ 508 nm). The photogenerated electrons are readily collected by the FTO electrode due to the energetically favorable landscape depicted in Figure 1f (perovskite/rGO (or PCBM)/FTO/Cu).[34,36] These photoelectrons accumulate on the counter-electrode through the external circuit (Figure 2e, photocharging), and we hypothesize that in the intercalation regime (low discharge), the photogenerated holes provide sufficient repulsion to drive Li-ions out of the perovskite matrix. This could then induce the photocharging of the battery as sketched in Figure 2e. The blend of perovskite with rGO/PCBM provides extensive conducting pathways through grain boundaries and interfaces, however short carrier lifetimes (~200 ps) and short diffusion lengths (<100 nm) of electrons and holes in 2D perovskites mean most either recombine or are trapped.[37] At lower discharges in the conversion region, we also observe some recharging (see Supporting Information, Figure S4), which may be due to residual intercalation effects, or due to the photogenerated holes reacting with the lithium iodide (LiI) to form Li^+:

$$2LiI + 2h^+ \rightarrow 2Li^+ + I_2 \tag{2}$$

The Li^+ is further reduced at the counter electrode by the accumulated photoelectrons ($Li^+ + e^- \rightarrow Li$), thus balancing the total photo generated carriers and inducing photocharging of the battery as sketched in Figure 2e. The capacity fading observed in the charge−discharge curves of the photobatteries (see Figure 2b,c), is probably due to a number of different factors including possibly deterioration of the material morphology during charging and discharging, the formation of insulating solid-electrolyte-interfaces (SEI) and the formation of poorly reversible lead metal Pb(*m*) (see chemical reaction 1). The photoinactive Pb(*m*) can alloy with Li to form Li_xPb ($0 < x < 4.4$) resulting in large volume increase and likely cracking and crumbling of the material.[38] This results in the loss of electrical contacts and hinders the reversibility of the reaction with Li, hence causes further capacity fading. Nevertheless, our system is relatively stable compared to other solar-chargeable energy storage devices,[11,13,15,16] and further improvements are possible by replacing Pb in the perovskite structure with other metals, such as Sn, Bi to provide better battery cycling. We note changes in elemental composition of the perovskite (in both 2D and 3D perovskites) cause changes in the optical band gap, which will change the performance of the photobattery. Perovskite photobatteries with alternative compositions should follow similar energy storage mechanisms and this may enable further device optimization. Overall, the above analysis underpins the unique capability of CHPI to combine both energy storage and photocharging mechanisms in the same material. This may lead to entirely new application domains for perovskites.

To date, batteries rely on external power sources to charge them. Our work demonstrates that highly photoactive 2D lead halide perovskites can simultaneously store energy and recharge by light. This paves the way for more compact integrated off-grid energy sources, which could profit in the longer term from fewer internal losses and lower weight than present separate solar cell/battery solutions. Our photobattery devices already show efficiencies comparable to those of electrodes using mixtures of solar cells and batteries and storage capacities of 100 mAh/g. Further, these materials can be solution processed which leads to straightforward scale-up strategies once more research is conducted to enhance their efficiency and stability.

Experimental Section.

Methods. Materials. The following chemicals were purchased from Sigma-Aldrich: Lead iodide (PbI_2), lead bromide ($PbBr_2$), hydroiodic acid (HI), hydrobromic acid (HBr), cyclo-hexyl-ethylamine ($C_6H_9C_2H_4NH_2$), reduced graphene oxide (rGO), electrochemical grade propylene carbonate, ethylene carbonate, diethyl carbonate, *N*-methyl-2-pyrrolidone, polyvinylidene fluoride (PVDF), and metal foils (Al, Cu, and Li). Polypropylene layers were purchased from Cell Guard. The phenyl-C61 butyric acid methyl ester (PCBM) of >99.5% purity grade was purchased from Solenne B.V.

Synthesis of Perovskites. The synthesis of 2D perovskite is performed by using a sol−gel method reported previously.[24,39] First ($C_6H_9C_2H_4NH_3$)X (X = I or Br) was synthesized from the mixture of 1:1 molar ratio of aqueous solutions of HX (HI or HBr) and cyclo-hexyl-ethylamine ($C_6H_9C_2H_4NH_2$) (100 °C and stirring at 2000 rpm). The precipitate from the reactant solution is separated and then washed with diethyl ether. To synthesize 2D perovskites ($(C_6H_9C_2H_4NH_3)_2PbX_4$), stoichiometric amounts of ($C_6H_9C_2H_4NH_3$)X and corresponding lead halide (PbI_2 or $PbBr_2$) were dissolved in *N,N*-dimethylformamide (DMF) (the resultant compounds are referred to as CHPI and CHPB, respectively). Perovskite powder is extracted from the above prepared solution by drying overnight in a vacuum oven at 60 °C.

Preparation of Electrodes. Perovskite photobattery electrodes were prepared by using different additives, rGO and PCBM. For both additives, lead halide perovskites are made following a similar recipe. 10 milligrams of rGO or PCBM is dissolved in 1 mL *N*-methy-2-pyrrolidone (NMP, in glovebox) and sonicated for 1 h. 85 milligrams of perovskite is dissolved in the same solution and stirred overnight. Then, 5 mg of polyvinylidene fluoride (PVDF) binder is added followed by 2 h of stirring. CHPI electrodes using PCBM/PVDF as additives are referred to as **B1** and rGO/PVDF as **B2** respectively. Both **B1** and **B2** were transferred in a glovebox to prepare the electrodes. 60 μl of **B1** or **B2** is drop-casted on precleaned and UV-ozone treated FTO substrates and left on a hot-plate for drying overnight at 45 °C. All devices are made on FTO substrates with an area of 1.0 cm × 1.5 cm.

Fabrication of the Photobatteries. Perovskite photobatteries are assembled in an Ar-filled glovebox. Al-metal foil and Li-metal foil (25 μm) are stacked on stainless steel (SS) disks. Whatman borosilicate paper, soaked with 1 M $LiPF_6$ as electrolyte, is placed on Li-metal as a separator. On top of the separator, the perovskite electrodes with a Cu-foil extended electrode are gently flipped and covered with another glass slide (2.5 cm × 3.7 cm) to hold all layers together. Finally, the edges were sealed and clips were used to maintain the interfacial contacts between all components of device.

Characterizations. All photobattery measurements were performed in air by using a Biologic VMP-3 galvanostat. For photocharging, an LED-based broadband ($\lambda \sim 420-650$ nm, intensity ~100 mW/cm^2) source is used for irradiation. Open circuit voltage (OCV) is measured to obtain the photocharge and discharge potential curves. For discharge, the photobattery is connected to either a resistor of 21.5 kΩ load or a commercial 3 V white light LED. A 447 nm diode laser is coupled to an Olympus BX-51 microscope for confocal PL measurements. For PL imaging, deep UV (300 nm, Thorlabs-M300L4) and UV (365 nm, Thorlabs-M365L2) mounted LEDs are used. For post-mortem analysis, the photobatteries are opened in an Ar-glovebox and dried overnight at 40 °C. The XRD measurement are performed on a Bruker D8, Raman on a Renishaw InVia Raman Microscope, and FTIR measurements on a PerkinElmer Frontier.

■ ASSOCIATED CONTENT

Ⓢ Supporting Information

The Supporting Information is available free of charge on the ACS Publications Web site at DOI: The Supporting Information is available free of charge on the ACS Publications website at DOI: 10.1021/acs.nanolett.7b05153.

Additional figures and references (PDF)

■ AUTHOR INFORMATION

Corresponding Authors

*E-mail: sa754@cam.ac.uk.
*E-mail: mfld2@cam.ac.uk.

ORCID

Jeremy J. Baumberg: 0000-0002-9606-9488
Michael De Volder: 0000-0003-1955-2270

Present Address

(S.A.) Centre for Nanoscience and Nanotechnology, Jamia Millia Islamia (A Central University), New Delhi, India 110025. E-mail: sahmad28@jmi.ac.in.

Notes

The authors declare no competing financial interest.

■ ACKNOWLEDGMENTS

Authors acknowledge support from Dr. A. Sadhanala, Optoelectronics Group, and Marie-Elena Kleemann, Nanophotonics Centre, for assistance with measurements. This work was funded by an ERC Starting Grant (HIENA-337739), ERC (LINASS, 320503), and EPSRC (EP/L027151/1, EP/N016920/1).

■ REFERENCES

(1) Haight, R.; Haensch, W.; Friedman, D. *Science* **2016**, *353*, 124−125.

(2) Ahmad, S.; Copic, D.; George, C.; De Volder, M. *Adv. Mater.* **2016**, *28*, 6705−6710.

(3) Chen, J.; Huang, Y.; Zhang, N.; Zou, H.; Liu, R.; Tao, C.; Fan, X.; Wang, Z. L. *Nat. Energy* **2016**, *1*, 16138.

(4) Zhou, G.; Li, F.; Cheng, H.-M. *Energy Environ. Sci.* **2014**, *7*, 1307−1338.

(5) Zhou, G.; Sun, J.; Jin, Y.; Chen, W.; Zu, C.; Zhang, R.; Qiu, Y.; Zhao, J.; Zhuo, D.; Liu, Y.; Tao, X.; Liu, W.; Yan, K.; Lee, H. R.; Cui, Y. *Adv. Mater.* **2017**, *29*, 1603366.

(6) Zhang, N.; Chen, J.; Huang, Y.; Guo, W.; Yang, J.; Du, J.; Fan, X.; Tao, C. *Adv. Mater.* **2016**, *28*, 263−269.

(7) Vlad, A.; Singh, N.; Galande, C.; Ajayan, P. M. *Adv. Energy Mater.* **2015**, *5*, 1402115.

(8) Xu, J.; Chen, Y.; Dai, L. *Nat. Commun.* **2015**, *6*, 8103.

(9) Xu, J.; Wu, H.; Lu, L.; Leung, S.-F.; Chen, D.; Chen, X.; Fan, Z.; Shen, G.; Li, D. *Adv. Funct. Mater.* **2014**, *24*, 1840−1846.

(10) Méndez, M. A.; Peljo, P.; Scanlon, M. D.; Vrubel, H.; Girault, H. H. *J. Phys. Chem. C* **2014**, *118*, 16872−16883.

(11) Miyasaka, T.; Ikeda, N.; Murakami, T. N.; Teshima, K. *Chem. Lett.* **2007**, *36*, 480−487.

(12) Thimmappa, R.; Paswan, B.; Gaikwad, P.; Devendrachari, M. C.; Makri Nimbegondi Kotresh, H.; Rani Mohan, R.; Pattayil Alias, J.; Thotiyl, M. O. *J. Phys. Chem. C* **2015**, *119*, 14010−14016.

(13) Paolella, A.; Faure, C.; Bertoni, G.; Marras, S.; Guerfi, A.; Darwiche, A.; Hovington, P.; Commarieu, B.; Wang, Z.; Prato, M.; Colombo, M.; Monaco, S.; Zhu, W.; Feng, Z.; Vijh, A.; George, C.; Demopoulos, G. P.; Armand, M.; Zaghib, K. *Nat. Commun.* **2017**, *8*, 14643.

(14) Nguyen, O.; Courtin, E.; Sauvage, F.; Krins, N.; Sanchez, C.; Laberty-Robert, C. *J. Mater. Chem. A* **2017**, *5*, 5927−5933.

(15) Nagai, H.; Sato, M. Highly Functionalized Lithium-Ion Battery. In *Alkali-ion Batteries*; InTech, 2016; Chapter 6.

(16) Nagai, H.; Suzuki, T.; Takahashi, Y.; Sato, M. *Funct. Mater. Lett.* **2016**, *09*, 1650046.

(17) Saliba, M.; Matsui, T.; Domanski, K.; Seo, J.-Y.; Ummadisingu, A.; Zakeeruddin, S. M.; Correa-Baena, J.-P.; Tress, W. R.; Abate, A.; Hagfeldt, A.; Gratzel, M. *Science* **2016**, *354*, 206−209.

(18) Akkerman, Q. A.; Gandini, M.; Di Stasio, F.; Rastogi, P.; Palazon, F.; Bertoni, G.; Ball, J. M.; Prato, M.; Petrozza, A.; Manna, L. *Nat. Energy* **2016**, *2*, 16194.

(19) Stranks, S. D.; Snaith, H. J. *Nat. Nanotechnol.* **2015**, *10*, 391−402.

(20) Xia, H.-R.; Sun, W.-T.; Peng, L.-M. *Chem. Commun.* **2015**, *51*, 13787−13790.

(21) Ahmad, S.; Prakash, G. V. *J. Nanophotonics* **2014**, *8*, 083892.

(22) Ahmad, S.; Kanaujia, P. K.; Beeson, H. J.; Abate, A.; Deschler, F.; Credgington, D.; Steiner, U.; Prakash, G. V.; Baumberg, J. *ACS Appl. Mater. Interfaces* **2015**, *7*, 25227−25236.

(23) Cao, D. H.; Stoumpos, C. C.; Farha, O. K.; Hupp, J. T.; Kanatzidis, M. G. *J. Am. Chem. Soc.* **2015**, *137*, 7843−7850.

(24) Safdari, M.; Svensson, P. H.; Hoang, M. T.; Oh, I.; Kloo, L.; Gardner, J. M. *J. Mater. Chem. A* **2016**, *4*, 15638−15646.

(25) Tai, Q.; You, P.; Sang, H.; Liu, Z.; Hu, C.; Chan, H. L. W.; Yan, F. *Nat. Commun.* **2016**, *7*, 11105.

(26) Jiang, Q.; Chen, M.; Li, J.; Wang, M.; Zeng, X.; Besara, T.; Lu, J.; Xin, Y.; Shan, X.; Pan, B.; Wang, C.; Lin, S.; Siegrist, T.; Xiao, Q.; Yu, Z. *ACS Nano* **2017**, *11*, 1073−1079.

(27) Cabana, J.; Monconduit, L.; Larcher, D.; Palacín, M. R. *Adv. Mater.* **2010**, *22*, E170−E192.

(28) Zhuang, G. V.; Yang, H.; Blizanac, B., Jr.; Ross, P. N. *Electrochem. Solid-State Lett.* **2005**, *8*, A441−A445.

(29) Zhao, X.; Park, N.-G. *Photonics* **2015**, *2*, 1139−1151.

(30) Dawson, J. A.; Naylor, A. J.; Eames, C.; Roberts, M.; Zhang, W.; Snaith, H. J.; Bruce, P. G.; Islam, M. S. *ACS Energy Lett.* **2017**, *2*, 1818−1824.

(31) Billing, D. G.; Lemmerer, A. *Acta Crystallogr., Sect. C: Cryst. Struct. Commun.* **2006**, *62*, m269−m271.

(32) Ahmad, S.; Kanaujia, P. K.; Niu, W.; Baumberg, J. J.; Vijaya Prakash, G. *ACS Appl. Mater. Interfaces* **2014**, *6*, 10238−10247.

(33) Ishihara, T.; Takahashi, J.; Goto, T. *Phys. Rev. B: Condens. Matter Mater. Phys.* **1990**, *42*, 11099−11107.

(34) Ishihara, T. *J. Lumin.* **1994**, *60−61*, 269−274.

(35) Dou, L.; Wong, A. B.; Yu, Y.; Lai, M.; Kornienko, N.; Eaton, S. W.; Fu, A.; Bischak, C. G.; Ma, J.; Ding, T.; Ginsberg, N. S.; Wang, L. W.; Alivisatos, A. P.; Yang, P. *Science* **2015**, *349*, 1518−21.

(36) Tsai, H.; Nie, W.; Blancon, J.-C.; Stoumpos, C. C.; Asadpour, R.; Harutyunyan, B.; Neukirch, A. J.; Verduzco, R.; Crochet, J. J.; Tretiak, S.; Pedesseau, L.; Even, J.; Alam, M. A.; Gupta, G.; Lou, J.; Ajayan, P. M.; Bedzyk, M. J.; Kanatzidis, M. G.; et al. *Nature* **2016**, *536*, 312−316.

(37) Milot, R. L.; Sutton, R. J.; Eperon, G. E.; Haghighirad, A. A.; Martinez Hardigree, J.; Miranda, L.; Snaith, H. J.; Johnston, M. B.; Herz, L. M. *Nano Lett.* **2016**, *16*, 7001−7007.

(38) Martos, M.; Morales, J.; Sánchez, L. *Electrochim. Acta* **2003**, *48*, 615−621.

(39) Mitzi, D. B. Synthesis, Structure, and Properties of Organic-Inorganic Perovskites and Related Materials; *Progress in Inorganic Chemistry*; John Wiley & Sons, Inc, 2007; Vol. *48*, pp 1−121.

DOI: 10.1021/acs.nanolett.7b05153
Nano Lett. XXXX, XXX, XXX−XXX